Medical Engineering and Physics 65 (2019) 24–30

Contents lists available at ScienceDirect

Medical Engineering and Physics

journal homepage: www.elsevier.com/locate/medengphy

Numerical model of aqueous humor drainage: effects of collector channel position

G.J. Martínez Sánchez[a], C. Escobar del Pozo[a,*], J.A. Rocha Medina[b]

[a] Faculty of Mechanical and Electrical Engineering, Carretera Km 9 Colima-Coquimatlán, C.P. 28400 Colima, México
[b] North Central Hospital PEMEX, Marina Nacional No. 329, Col. Petroleos Mexicanos, C.P. 11311, Ciudad de Mexico

ARTICLE INFO

Article history:
Received 25 October 2017
Revised 5 November 2018
Accepted 16 December 2018

Keywords:
Anterior chamber
Glaucoma
Collector channels
Intraocular pressure
Finite element method
OpenFOAM

ABSTRACT

Glaucoma is a progressive and a degenerative eye disease that gradually deteriorates the vision. The origin of glaucoma is still under debate. Recent studies report that 50% of the aqueous humor outflow resistance resides on collector channels and Schlemm's canal (SC). This paper provides a descriptive analysis of the aqueous humor outflow through the anterior chamber, the trabecular meshwork (TM) and the SC. The aim of this work is to determine the influence of the collector channels position on the intraocular pressure (IOP) and its contribution to the development of glaucoma. Pressure and wall shear stress distributions are presented for four cases. The first case has an arrangement of collector channels according to micro CT (Gong and Francis, 2014). The remaining cases have an symmetrical distribution; case 2 has all open quadrants (AOQ), cases 3 have three quadrants completely open and just one quadrant semi closed (SCQ), and finally cases 4 consider that a quadrant is completely closed (CQ). Symmetrical and micro CT cases have 29 collector channels. The results show that the position and the opening of the collector channels have a strong influence on the IOP.

1. Introduction

Glaucoma is the second leading cause of blindness in the world [1], and is commonly associated with an intraocular pressure (IOP) increase. However, the causes of this neuropathy are still under discussion. The pressure rise is related with an unbalance between the inflow and the drainage of aqueous humor, that under normal conditions are the same and is about 2 μl to 2.5 μl per minute [2]. The drainage of this fluid is mainly through two pathways: the TM, located in the angle between the cornea and the iris; and the second is the uveoscleral, which is a structure located in the ciliary body. The trabecular pathway drains from 75% to 90% of aqueous humor flow; meanwhile, the uveoscleral pathway drains from 10% to 25% of the total of the aqueous humor [3].

Even though is well known that elevated IOP is a risk factor to develop glaucoma, is not necessarily the cause. As far as the authors know, three hypotheses have gained acceptance in recent years. The first hypothesis states that the IOP increment is linked to an elevated aqueous drainage resistance caused by pathological changes in the TM [4–6]. The second theory states that the pressure increase occurs in the internal layer of the SC due to the formation of giant vacuoles, these giant vacuoles modify the geometry of the SC, at the same time these vacuoles offer a resistance to the flow of the AH, this is due to the fact that the vacuoles stored AH during a small period of time [7]. Finally, the third theory indicates that the resistance to the aqueous humor flow is increased by the closure of the collector channels, the increase in resistance to flow is attributed to the reduction of the area due to the number of collecting channels that are interconnected with the venous system [1,8]. Neither of them have been confirmed or denied.

Mathematical models and numerical methods have been developed to describe the fluid dynamics of the aqueous humor. Ismail and Fitt [9] did a mathematical model explaining the flow of the aqueous humor through Schlemms canal taking into account the deformation of the TM related with IOP. The same authors used a regular perturbation method to solve the model using a constant permeability of the TM.

They obtained the relation between the deformation of the TM and the pressure within the anterior chamber; if the amount of the aqueous humor flowing across TM is negligible the IOP rises dramatically and blindness will inevitably result. Another mathematical model was made by Fitt and Gonzalez [10] to analyse different mechanisms that produce aqueous humor flow in the anterior chamber: (i) buoyancy effects due temperature differences between the anterior surface of the cornea and the iris, (ii) the aqueous humor flow generated by the ciliary body, (iii) the

* Corresponding author.
E-mail address: cescobar@ucol.mx (C. Escobar del Pozo).

https://doi.org/10.1016/j.medengphy.2018.12.022
1350-4533/

aqueous humor flow generated by interaction between buoyancy and gravity effects, (iv) the aqueous humor flow by phakodenesis and (v) the aqueous humor flow due by Rapid Eye Movement (REM). Their results show a maximum velocity for the aqueous humor flow at the anterior chamber of 7.5 $\times 10^{-6}\, m \cdot s^{-1}$.

Numerical efforts have been made to understand the aqueous humor dynamics. Repetto et al. [11] studied the fluid dynamic effects of an iris-fixated lens in the anterior chamber, using openFOAM ® software. Wall shear stresses, on the cornea and the iris, are obtained as well as velocities and pressure distribution in the anterior chamber. They showed that the intraocular lens has little influence on aqueous humor dynamics. Karampatzakis and Samaras [12] described the aqueous humor flow inside the anterior chamber considering the heat transfer between the cornea and the interior of the eye employing Comsol Multiphysics 3.5a (COMSOL AB, Stockholm, Sweeden). They calculated a maximum velocity for the aqueous humor flow within the anterior chamber of 3.36 $\times 10^{-4}\, m \cdot s^{-1}$. Moreover, Tiang and Ooi [13] did a further study of the aqueous humor hydrodynamics under external heat sources using Comsol Multiphysics 3.5a (COMSOL AB, Stockholm, Sweeden). Two types of heat sources were examined. Namely, exposure to ultra-high-frequency EM waves (750 MHz and 1.5 GHz) and surface heating due to IR irradiation. Their results demonstrate a maximum velocity for the aqueous humor flow of 3 $\times 10^{-4}\, m \cdot s^{-1}$ in normal thermophysiological conditions is obtained and a maximum velocity of 3.9 $\times 10^{-4}\, m \cdot s^{-1}$ subjected to the heat sources above named.

Villamarin et al. [14] did a 3D simulation of the aqueous humor using ANSYS CFX (ANSYS Inc., Canonsburg, PA, USA). They obtained velocities, pressures and wall shear stresses under normal and pathological conditions, particularly glaucoma conditions, taking into account collector channels. The authors obtained an average velocity of 7 $\times 10^{-6}\, mm \cdot s^{-1}$ within the anterior chamber, an IOP of 1799.85 *Pa* for a healthy eye and 3599.69 *Pa* for eye under glaucoma conditions. According to Gong and Hann [1,8], the collector channels play an important role in regulating the IOP. In this regard, a recent numerical research shows that the position of the collector channels could have an impact on the pressure inside of the SC [15].

New evidence shows that the aqueous humor drainage has preferential quadrants, in particular nasal and inferior quadrants [16]. This result suggests that the collector channels position could play a major role in eye pathology. Therefore, the aims of this study are to determine the influence of the collector channels distribution on the IOP, and to determine the pressure and wall shear stress in the SC. A numerical simulation is developed, using a model based on a human eye as a reference case; and 3 different distributions are proposed: symmetrical case, semi closed quadrant and closed quadrant.

2. Mathematical model

2.1. Anterior chamber model

The anterior chamber model used in this paper was built based on the human eye model geometry described by Villamarin et al. [14]. The anterior chamber has a diameter of 11.5×10^{-3} m and 5×10^{-3} m height. The SC is considered with a rectangular cross section, base of 300 μm and thickness of 100 μm. Finally, each collector channel has a diameter of 25 μm and a length of 100 μm. Geometrical details of the TM, the SC and the collector channels are available at [3,17,18]. The model comprises the following domains: the anterior chamber, the TM, the SC and the collector channels as is shown in Fig. 1.

An axial symmetric eye model is assumed, in order to study the different flows patterns induced by the collector channels

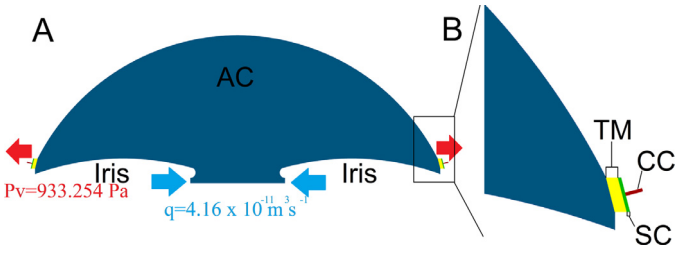

Fig. 1. Domains of the anterior chamber model: Anterior chamber in blue (AC), trabecular meshwork in yellow (TM), Schlemm's canal in green (SC) and collector channels in red (CCs). (A) Slice of the anterior chamber model; inlet in blue arrows and outlet in red arrows. (B) Close up of the slice. (For interpretation of the references to color in this figure legend, the reader is referred to the web version of this article.)

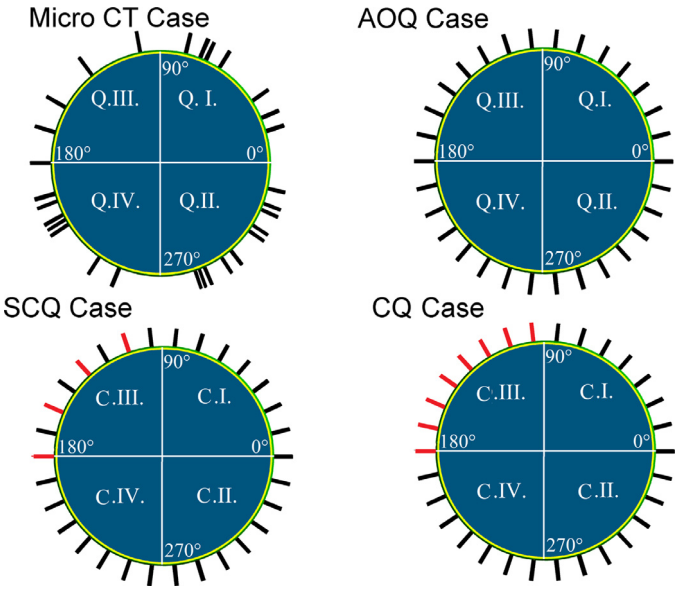

Fig. 2. Cases studied. In red and black lines, the position of collector channels. In red line close collector channels and in black line the open collector channels. (For interpretation of the references to color in this figure legend, the reader is referred to the web version of this article.)

position instead of the patterns promotes by asymmetries of the eye geometry. Moreover, the results obtained by [14] did not show significant variations form the axial symmetric case.

The model takes into account 4 different cases and each case have been broken down into quadrants. Case 1 has 29 collector channels and the distribution of these channels was obtained from a micro computerized tomography (CT) [1]. The remaining cases have 29 collector channels and a symmetrical distribution. The case 2 has all open quadrants (AOQ), all collector channels are open. Cases 3 has three quadrants completely open and just one quadrant semi closed (SCQ), that means that the SCQ has 4 collector channels open and 4 channels closed. The last case considers that a quadrant is completely closed (CQ); meanwhile, the other quadrants are open. Each case is shown in Fig. 2, in which the red channels means that are closed ones.

2.2. Governing equations

The aqueous humor is a clear fluid that, carries on nutrients to the anterior chamber and keep clear the medium for letting through the light. In this paper, the aqueous humor is assumed like a Newtonian fluid with constant properties, since there are no changes in temperature. The equations that describe aqueous humor dynamics are the Navier–Stokes and mass conservation

Table 1
Properties of the aqueous humor and trabecular meshwork used in the fluid's simulation.

Property	Value	Reference
Trabecular meshwork permeability	$3 \times 10^{-16} m^2$	[15]
Aqueous humor density	$998.7\ kg \cdot m^{-3}$	[17]
Aqueous humor viscosity	$7.5 \times 10^{-4}\ Pa \cdot s$	[17]

equations. A steady state analysis is done, assuming that the aqueous humor is an incompressible liquid and neglecting the effects associated with gravity effects. The equations of motion of the aqueous humor in 3 dimensions are reduced to

$$\nabla \cdot \mathbf{v} = 0 \tag{1}$$

$$\rho(\mathbf{v} \cdot \nabla \mathbf{v}) = -\nabla p + \mu \nabla^2 \mathbf{v} \tag{2}$$

where ρ $[kg \cdot m^{-3}]$ is density of the aqueous humor; $\mathbf{v}$ $[m \cdot s^{-1}]$ is the velocity; p $[Pa]$ is the pressure and μ $[Pa \cdot s]$ is the dynamic viscosity of the aqueous humor.

The TM is assumed as a rigid and homogeneous porous medium with constant permeability. Darcy's law set out in Eq. (3) is used to define the permeability of the TM [19].

$$q = -\frac{K}{\mu} \cdot \nabla p \tag{3}$$

where q $[m^3 \cdot s^{-1}]$ is the volumetric flow rate, K $[m^2]$ is the permeability of the TM, μ $[Pa \cdot s]$ the viscosity of the aqueous humor and ∇p $[Pa \cdot m^{-1}]$ is the pressure gradient. The properties of the aqueous humor and the TM used in the simulation are shown in Table 1.

2.3. Boundary conditions

An inlet volumetric flow rate of $q = 4.16 \times 10^{-11} m^3 \cdot s^{-1}$ was imposed, according to Siggers and Ethier [2,20], at the entrance area, blue arrows in Fig 1. The cornea and the iris surfaces are rigid and fixed; no slip condition was considered between the aqueous humor and rigid walls. Finally a venous pressure, of 933.254 *Pa* [17] is proposed as outlet condition at the collector channels outlet, shown with red arrows in Fig. 1. In the porous medium a no slip condition was taken into account at the walls of the TM.

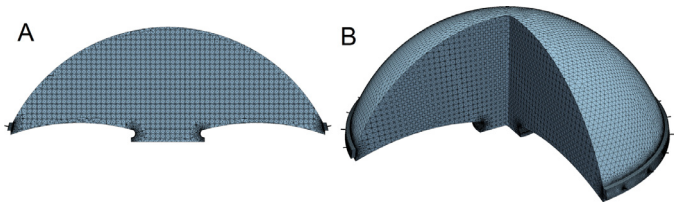

Fig. 4. Discretized of the anterior chamber model. (A) Sagittal views and (B) isometric view.

2.4. Numerical implementation

The anterior chamber model and the volumetric mesh were created with ICEM CFD software (ANSYS Inc., Canonsburg, PA, USA). The simulations were performed using the software OpenFOAM—5.0 ®, a partial differential equation calculator that utilizes the finite element method. In order to employ a minimum number of elements and reduce the compute time a mesh convergence test was necessary to identify the mesh independent solutions. The results are presented in Fig. 3A., that shows the convergence of the maximum velocity and Fig. 3B shown the convergence of the maximum pressure. The results are considered to be mesh independent when the percentage difference between two successive meshes is less than 0.5%. According to Fig. 3, the model requires 3,042,946 tetrahedral elements.

Fig. 4 shows the discretized model. Fig. 4A represents a slice of the model, a sagittal view. Fig. 4B shows an isometric view of the anterior chamber model part.

3. Results

In the present study, only the flow induced by aqueous production and drainage is considered. The obtained results are the anterior chamber pressure, the wall shear stresses on the iris and the cornea, and the wall shear stress on the wall of the SC. Wall shear stress is a relevant variable linked with endothelial cells function and cornea and iris cells detachment [1]; therefore, WSS could be used as a damage indicator or as a reference for normal conditions. Fig. 5 indicates the pressure contour in a slice plane located at the center of the volume for the symmetrical model and the channel collectors distribution of micro CT [1]. Any mean differences between the two cases in the IOP can be appreciated.

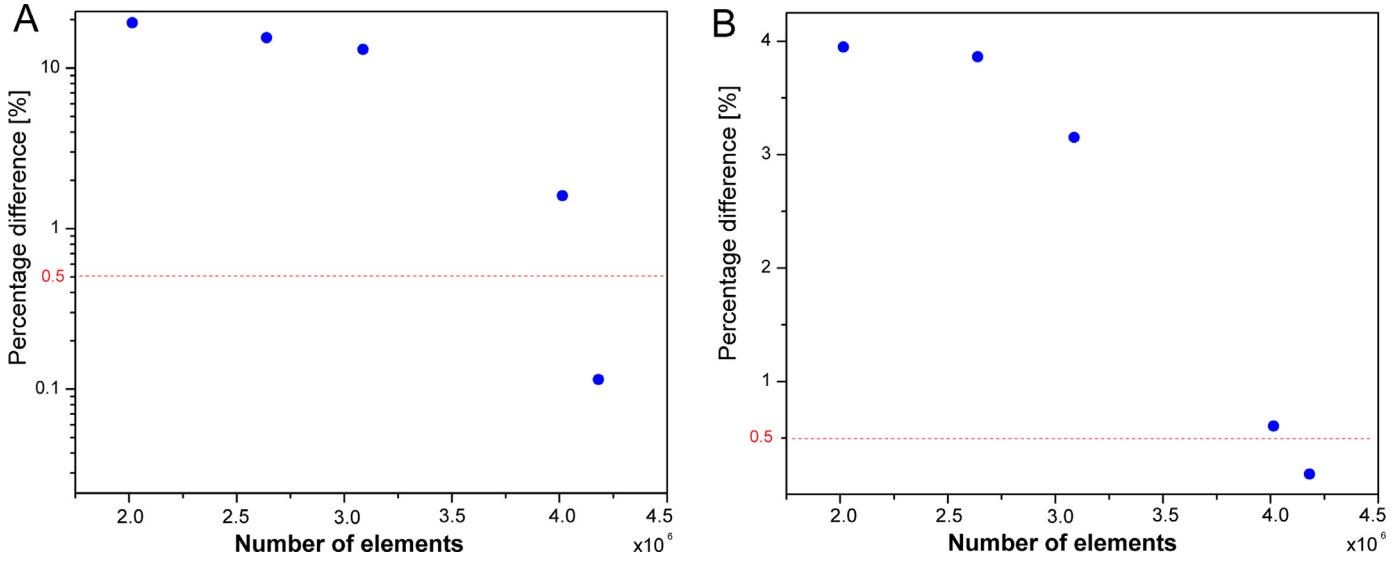

Fig. 3. Convergence plot for the (A) velocity and (B) pressure. Dotted line is the convergence threshold of 0.5%.

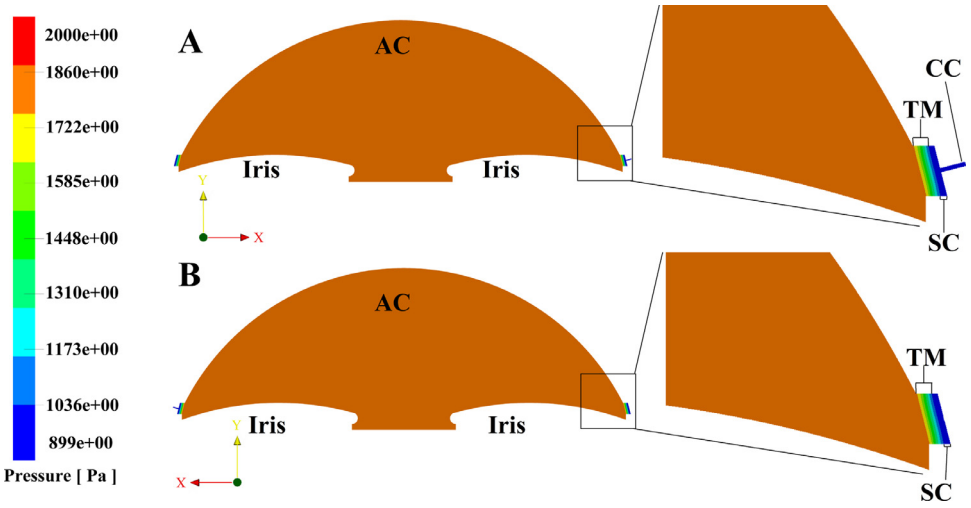

Fig. 5. Contour of pressure in the anterior chamber (AC), trabecular meshwork (TM), Schlemm's canal (SC) and collector channel (CC). (A) Symmetrical model, (B) Micro CT model.

Table 2
Pressure in the anterior chamber.

Study case	Volume average pressure [*Pa*]
Micro CT	1773.6
Symmetrical	1732.2
Semi closed quadrant	1777.2
Closed quadrant	1787.3

Table 3
Average wall shear stress.

Study case	Cornea [*Pa*]	Iris [*Pa*]	Schlemm's canal [*Pa*]
Micro CT	2.66×10^{-6}	3.61×10^{-6}	4.44×10^{-3}
Symmetrical	2.56×10^{-6}	3.55×10^{-6}	1.08×10^{-4}
Semi closed quadrant	4.54×10^{-6}	3.68×10^{-6}	6.28×10^{-3}
Closed quadrant	4.42×10^{-6}	3.7×10^{-6}	2.52×10^{-2}

Pressure distributions are illustrated in Fig. 5, as can be seen there is no difference between case A and case B in the pressure drop in the SC, neither in the collector channels. Furthermore, Table 2 shows the volume average pressure in the anterior chamber. Taking the Micro CT as the reference case, a pressure reduction of 2.3 % is observed for the symmetrical case; on the other hand, a pressure increment of 0.2 % and 0.8 % is obtained for semi closed and closed quadrant, respectively.

In Table 2 Micro CT and symmetrical case correspond to case AOQ, semi close quadrant represents case SCQ, and finally close quadrant corresponds CQ case of Fig. 2. Symmetrical case has the lowest average pressure, on the other hand close quadrant case has the highest average pressure. The difference between symmetrical case and Micro CT case is 41.4 Pa, the difference between symmetrical and semi close quadrant case is 45 Pa, and the difference between symmetrical case and close quadrant is 55.1 Pa. In close quadrant cases as well as semi close quadrant cases do not matter in which quadrant are the closed collector channels.

Figs. 6 to 8 show the wall shear stresses on the cornea, iris and SC, respectively. The results of all cases of close collector channels are similar between each other. Therefore, Figs. 6 to 8 show the characteristic case. The same behaviour is shown for semi close collector channels.

Figs. 6 and 7 do not have mean changes in the wall shear stress. Fig. 6 shows that the smallest wall shear stress is at the center of the cornea, and the maximum wall shear stress is at the edge of the cornea. The same behaviour is presented for all cases. The wall shear stress grows as it goes from the center to the edge of the cornea. Fig. 7 shows that the wall shear stresses decrease from the center to the peripheral border in radial direction, reaching the maximum value at the edge of the center. The same behaviour is presented for all cases. Apart from that, it is clear that the higher wall shear stresses are found near to the opening of the collector channels, as can be observed in Fig. 8. Area average wall shear stresses results of the 4 cases are presented in Table 3.

The symmetric case has the smallest average wall shear value of all cases in the cornea, the iris and the SC. On the other hand, the greatest average wall shear stress value in the cornea was calculated in the semi closed quadrant case, meanwhile for the cornea and the SC the greatest value was obtained in the closed quadrant case. As is shown in Table 3.

Pressure results at the center of SC are represented in Fig. 9. The micro tomography case, Micro CT case in Fig. 9, has the lowest average pressure, 950.12 Pa. Meanwhile, the CQ case has the greater average pressure, 965.19 Pa. It is clear that a closed quadrant results in increase average pressure of 1.6 % in contrast with the Micro CT case and a maximum pressure of 991.43 Pa, an 4.3 % increment from the average value. Fig. 9 also shows that the Micro CT has zones without collector channels, that are very similar to the SCQ case.

4. Discussion and conclusions

The permeability of the TM is critical in order to solve the drainage flow problem. For carrying out the numerical simulation of the TM permeability was determined through several simulations in order to obtain a volumetric flow rate reported normal physiologically. It is necessary, therefore, to define a proper value to carry out the numerical simulation. The TM permeability was determined through the model in ring shape [15]. The model took into account the SC and the TM, and a permeability was obtained of $3 \times 10^{-16} m^2$.

In order to validate the numerical simulation, the results for the symmetrical case were compared with those obtained by Villamarin et al. [14] is done. The cited work determined velocity profiles, pressure contours and wall shear stress in the SC from a reconstructed eye structure with a symmetrical collector channels distribution, taking into account 26 collector channels, a permeability value of $1.5 \times 10^{-15} m^2$, a volumetric flow rate of 3 µl per minute as inlet condition, and an outlet pressure of 7 mmHg. The

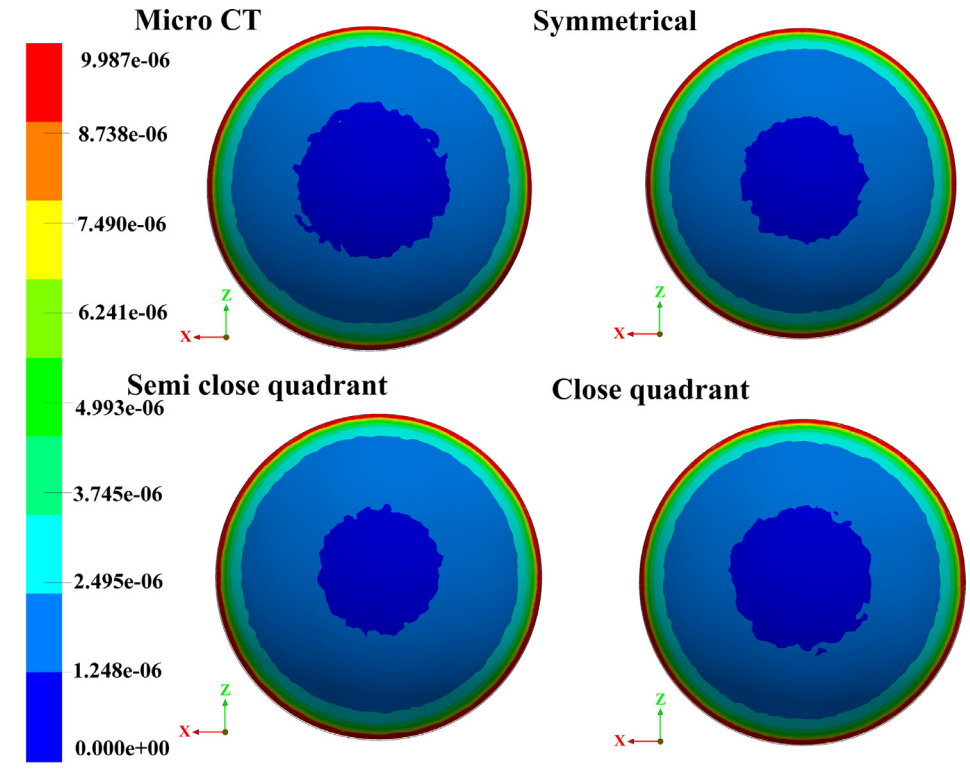

Fig. 6. Wall shear stress on the cornea.

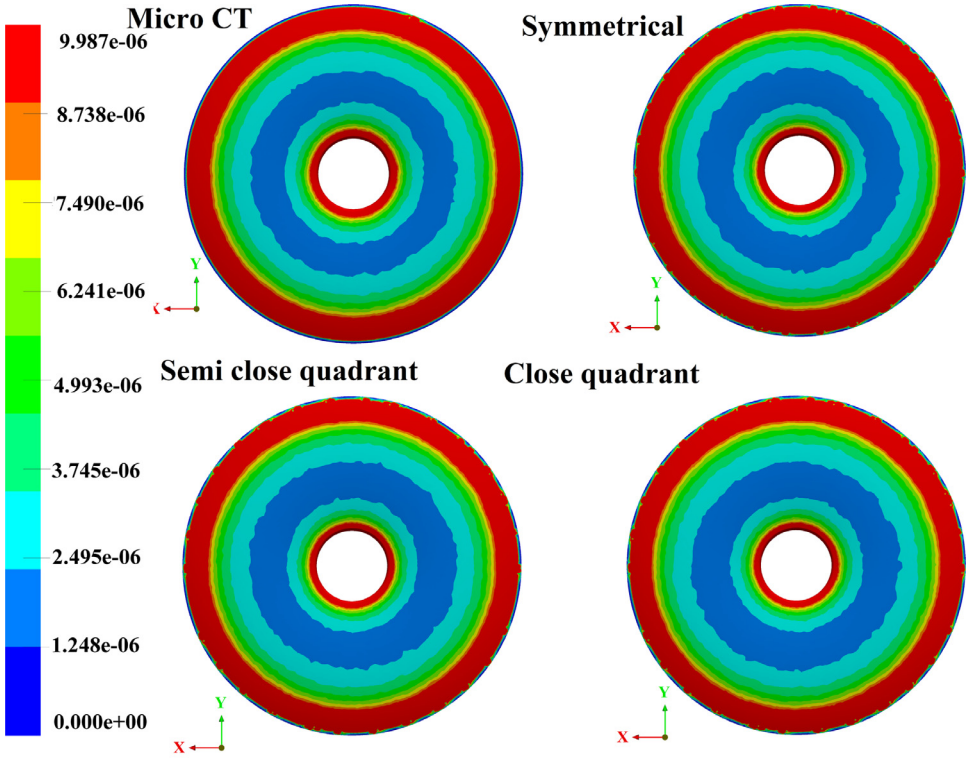

Fig. 7. Wall shear stress on the iris.

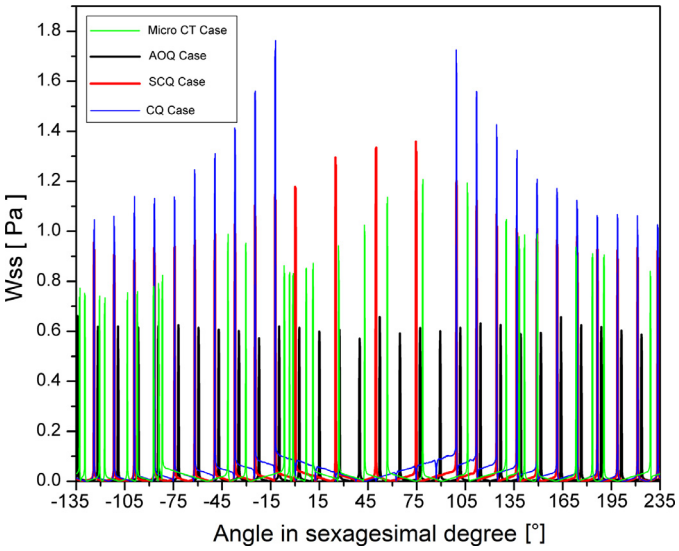

Fig. 8. Wall shear stress on the Schlemm's canal.

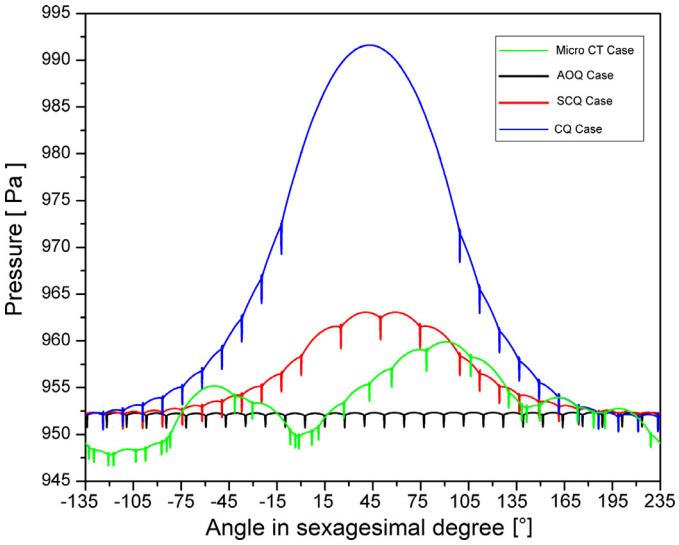

Fig. 9. Pressure in the center of the Schelmm's canal. It shows case 1, case 2 and CQ cases.

pressure difference in the anterior chamber between the cited paper and the presented results is of 1.6%; which validates our simulation process.

The anterior chamber model asserts that the IOP increases as the number of closed collector channels increases, no matter the quadrant. Semi close quadrant cases have leaped in pressure distribution, while closed quadrant cases have a uniform pressure distribution; although these last ones increase the pressure values. The results show that the position of the collector channels has an influence on the IOP, whereas the pressure increment does not represent a dangerous condition.

The pressure difference within the SC between the all open quadrant (AOQ) case with minimum pressure and closed quadrant (CQ) cases with a maximum pressure of the 3D geometry, is 1.47%. The pressure difference within the anterior chamber between of AOQ case and CQ cases is 0.81% while the shear stress difference on the iris of the same cases is 4.24%. The shear stress difference of cornea between the case with minimum effort (micro CT) and maximum effort (AOQ) is 69.72% and for the SC, the shear stress difference between the AOQ case and the semi-closed quadrant (SCQ) cases is 4447.33%. The obtained shear stresses on iris and cornea are the normal physiological range [21]. The differences in shear stresses in SC are due to the reduction of drainage area, and this changes could trigger aqueous humor flow regulation processes that are not taken into account in the present work that could lead to IOP variations and tissue damages.

The results showed an average pressure reduction of 2.3% between the Micro CT and symmetrical cases; also an increment of 3.18% between symmetrical and closed quadrant cases. According to [22,23] an IOP variation of 3% is not significant; however, is not possible to evaluate if this small IOP changes could promote damages in a long period of time and it is important to take into account that patients with glaucoma are sensitive to IOP variations [24].

To the authors' knowledge, no critical pressure values have been reported in SC. On account of no reference is known it is not possible to establish whether pressure or pressure variations are the cause of probable damages. Therefore, it is important in order to report slight variations in pressure. On the other hand, significant changes are observed in wall shear stresses in the cornea and in the Schelmm's canal; however, it is not possible to identify cell detachment or any other damaged caused by shear stresses. More experimental values need to be obtained to compare and to determine if the conditions presented in this paper promote pathology conditions.

According to with the descriptive results, collector channels play a major role in the shear stresses in SC, and its position modifies the IOP; however with the obtained results is not possible to determine its relevance. New studies of numerical simulations, taking into account a transitory state, are required in order to determine if the pressure variations induced by the distribution of the collector channels causes damages on eye structures, like iris, cornea, and the TM tissue. In addition, the present research shows the need for more studies *in vivo* to determine the normal distribution of the collector channels in humans in physiological and glaucoma conditions. Finally, more work needs to be done considering gravitational as well as buoyancy effects; which could increase the relevance of the position of the collector channels, due to the gravitational acceleration direction as well as a temperature gradient in a radial direction, considering the eye as a sphere.

Acknowledgments

GJ Martnez thanks the master degree scholarship supported by Consejo Nacional de Ciencia y Tecnologa (CONACYT) at Mexico.

Conflicts of interest

None.

Funding

This work was supported by Consejo Nacional de Ciencia y Tecnologa (CONACYT) [grant: 427822].

Ethical approval

Not required.

References

[1] Gong H, Francis A. Schlemm's canal and collector channels as therapeutic targets. In: Surgical Innovations in Glaucoma; 2014. p. 3–25.
[2] Siggers JH, Ethier CR. Fluid mechanics of the eye. Ann Rev Fluid Mech 2012;44:347–72.
[3] Dautriche CN, Xie Y, Sharfstein ST. Walking through trabecular meshwork biology: Toward engineering design of outflow physiology. Biotechnol Adv 2014;32(5):971–83.

[4] Ethier CR, Coloma FM, de Kater AW, Allingham RR. Retroperfusion studies of the aqueous outflow system. part 2: studies in human eyes. Investig Ophthalmol Vis Sci 1995;36(12):2466–75.
[5] Grant WM. Experimental aqueous perfusion in enucleated human eyes. Arch Ophthalmol 1963;69(6):783.
[6] Mäepea O, Bill A. Pressures in the juxtacanalicular tissue and Schlemm's canal in monkeys. Exper Eye Res 1992;54(6):879–83.
[7] Pedrigi RM, Simon D, Reed A, Stamer WD, Overby DR. A model of giant vacuole dynamics in human Schlemm canal endothelial cells. Exper Eye Res 2011;92(1):57–66.
[8] Hann CR, Vercnocke AJ, Bentley MD, Jorgensen SM, Fautsch MP. Anatomic changes in Schlemm's canal and collector channels in normal and primary open-angle glaucoma eyes using low and high perfusion pressures distal outflow pathway at low and high pressure. Investig Ophthalmol Vis Sci 2014;55(9):5834–41.
[9] Ismail Z., Fitt A.D.. Mathematical modelling of flow in Schlemm's canal and its influence on primary open angle glaucoma. Proceedings of the international conference on science & technology: applications in industry & education2008;.
[10] Fitt AD, Gonzalez G. Fluid mechanics of the human eye: aqueous humour flow in the anterior chamber. Bull Math Biol 2006;68(1):53–71.
[11] Repetto R, Pralits JO, Siggers JH, Soleri P. Phakic iris-fixated intraocular lens placement in the anterior chamber: Effects on aqueous flowphakic iris-fixated intraocular lens placement. Investig Ophthalmol Vis Sci 2015;56(5):3061–8.
[12] Karampatzakis A, Samaras T. Numerical model of heat transfer in the human eye with consideration of fluid dynamics of the aqueous humour. Phys Med Biol 2010;55(19):5653.
[13] Tiang KL, Ooi EH. Effects of aqueous humor hydrodynamics on human eye heat transfer under external heat sources. Med Eng Phys 2016;38(8):776–84.
[14] Villamarin A, Roy S, Hasballa R, Vardoulis O, Reymond P, Stergiopulos N. 3D simulation of the aqueous flow in the human eye. Med Eng Phys 2012;34(10):1462–70.
[15] Martínez GJ, Escobar C, Villa Velázquez CI. Influencia de la posición de los canales colectores en la presión intraocular. Revista Mexicana de Ingeniería Biomédica 2017;38(1):314–23.
[16] Cha EDK, Xu J, Gong L, Gong H. Variations in active outflow along the trabecular outflow pathway. Exper Eye Res 2016;146:354–60.
[17] Johnson MC, Kamm RD. The role of schlemm's canal in aqueous outflow from the human eye. Investig Ophthalmol Vis Sci 1983;24(3):320–5.
[18] Simón G. Trabeculoplastia con dos tipos de láser en gato, monos y humano: estudio morfológico con microscopía electrónica de barrido. Archivos de la Sociedad Española de Oftalmología 2006;81(9):527–36.
[19] Merchant BM, Heys JJ. Effects of variable permeability on aqueous humor outflow. Appl Math Comput 2008;196(1):371–80.
[20] Ethier CR, Kamm RD, Palaszewski BA, Johnson MC, Richardson TM. Calculations of flow resistance in the juxtacanalicular meshwork. Investig Ophthalmol Vis Sci 1986;27(12):1741–50.
[21] Joseph Antony S. Imaging shear stress distribution and evaluating the stress concentration factor of the human eye. Sci Rep 2015;5(8899). doi:10.1038/srep08899.
[22] Moses RA, Grodzki WJ Jr, Etheridge EL, Wilson CD. Schlemm's canal: the effect of intraocular pressure.. Investig Ophthalmol Vis Sci 1981;20(1):61.
[23] Lee JW, Park H, Choi JH, Lee HJ, Moon SW, Kang JH, et al. Short-term changes of intraocular pressure and ocular perfusion pressure after intravitreal injection of bevacizumab or ranibizumab. BMC Ophthalmol 2016;16(1):69. doi:10.1186/s12886-016-0255-8.
[24] Sit AJ. Intraocular pressure variations: causes and clinical significance. Can J Ophthalmol 2014;49(6):484–8. doi:10.1016/j.jcjo.2014.07.008. GLAUCOMA MANAGEMENT; http://www.sciencedirect.com/science/article/pii/S0008418214002567.